Xu *et al. Microstructures* **2025**, *5*, 2025037
DOI: 10.20517/microstructures.2024.186

Microstructures

Research Article

Open Access

Check for updates

Lignin/graphene oxide composite coating loaded with zinc ions and its photothermal conversion and self-healing anticorrosion properties

Chang-An Xu[1,#], Wenzi Liang[2,#], Peiping Hong[1], Yang Hu[3], Zhuohong Yang[3], Hao Pang[1]

[1]Institute of Chemical Engineering, Guangdong Academy of Sciences, Guangzhou 510665, Guangdong, China.
[2]Shantou University Medical College, Shantou University, Shantou 515041, Guangdong, China.
[3]Key Laboratory for Bio-based Materials and Energy of Ministry of Education, College of Materials and Energy, South China Agricultural University, Guangzhou 510642, Guangdong, China.
[#]Authors contributed equally.

Correspondence to: Dr. Chang-An Xu, Institute of Chemical Engineering, Guangdong Academy of Sciences, No. 318 Chebei West Road, Tangxia, Tianhe District, Guangzhou City, Guangzhou 510665, Guangdong, China. E-mail: xuchangan@gdcri.com; Dr. Zhuohong Yang, Key Laboratory for Bio-based Materials and Energy of Ministry of Education, College of Materials and Energy, South China Agricultural University, No. 483 Wushan Road, Tianhe District, Guangzhou City, Guangzhou 510642, Guangdong, China. E-mail: yangzhuohong@scau.edu.cn; Dr. Hao Pang, Institute of Chemical Engineering, Guangdong Academy of Sciences, No. 318 Chebei West Road, Tangxia, Tianhe District, Guangzhou City, Guangzhou 510665, Guangdong, China. E-mail: panghao@gdcri.com

How to cite this article: Xu, C. A.; Liang, W.; Hong, P.; Hu, Y.; Yang, Z.; Pang, H. Lignin/graphene oxide composite coating loaded with zinc ions and its photothermal conversion and self-healing anticorrosion properties. *Microstructures* **2025**, *5*, 2025037. https://dx.doi.org/10.20517/microstructures.2024.186

Received: 27 Dec 2024 **First Decision:** 8 Feb 2025 **Revised:** 9 Feb 2025 **Accepted:** 14 Feb 2025 **Published:** 11 Apr 2025

Academic Editor: Shiqing Deng **Copy Editor:** Fangling Lan **Production Editor:** Fangling Lan

Abstract

At present, using biomass materials to modify graphene oxide (GO) to enhance the anticorrosion performance of coatings meets the requirements of future sustainable development. In order to endow lignin/GO coatings with self-healing function to reduce maintenance costs and avoid accidents caused by material corrosion failure, this work utilized electrostatic interactions to load zinc ions onto lignin/GO (Zn@LGO). Experimental results indicated that the cured coating exhibited both self-healing anticorrosion and photothermal conversion properties. When the content of Zn@LGO was 0.4 wt%, the surface temperature of the cured coating rose to 139.2 °C after 180 s of near-infrared radiation. The cured coating was left for 100 days in salt water, the $Z_{0.01Hz}$ value of coating VER-3 was up to 1.3 × 10^9 Ω cm^2, which was two orders of magnitude higher than that of pure resin coating, and fewer corrosion products were observed on the metal surface. The scratch test showed that the damaged coating was soaked in 3.5 wt% sodium chloride for 72 h; the charge transfer impedance of coating VER-3 was 2.61 × 10^4 Ω cm^2,

which was one order of magnitude higher than that of pure resin coating. This was mainly because during metal corrosion, the hydroxide generated by the combination of hydroxide ions at the cathode and zinc ions covered the damaged area of cured coating, hindering the penetration of the corrosive medium. All in all, this research promoted the application of lignin, and also provided a reference for the design of composite coatings with both photothermal conversion and self-healing anticorrosion properties.

Keywords: Self-healing, microstructure, anticorrosive, coating, graphene oxide, lignin

INTRODUCTION

Graphene oxide (GO) contains epoxy, hydroxyl, carbonyl, and carboxyl groups, and these rich active sites provide the possibility of modifying GO[1]. Coupled with the excellent physical barrier properties of GO to oxygen, water, and ions, it is frequently used as a reinforcing filler for coatings to improve their corrosion resistance[2-4]. However, due to the lack of organic self-healing groups in its structure, it lacks self-healing ability. In addition, due to the strong π-π interactions and van der Waals forces between GO, GO is prone to aggregation, resulting in poor compatibility and dispersion of GO in resin. This leads to the loss of metal protection for GO-based coatings before reaching their service life. Therefore, before adding GO to the resin, it is necessary to modify it to improve its dispersibility and compatibility in the resin, and endow it with self-healing properties.

Researchers believe that the surface modification or functionalization of GO by nanoparticles, organic molecules or polymers can greatly improve its dispersibility and compatibility[2,5-7]. According to existing literature, most of current materials for modified GO are petroleum-based products, which will seriously hinder the sustainable development of polymer materials based on petroleum-based raw materials[8,9]. With the global resource crisis and environmental pollution becoming increasingly prominent[10], the research community has begun to turn its attention to resource-rich biomass resources. Lignin is one of the most abundant green and renewable biomass resources in nature[11,12]. It is widely used in industry, light industry, and agriculture because of its non-toxic, carbon neutral, and large reserves characteristics. The molecular structure of lignin contains abundant polar groups and benzene ring structures, which can play a role in modifying and enhancing the performance of the material[13]. The benzene ring structure on the lignin can produce π-π interaction with GO, which can improve the dispersibility and compatibility of GO, and the corrosion resistance of GO-based coating is enhanced to ensure the safe service of the metal. In our previous study, GO was grafted with small molecular pyridine monomers and lignin. After treatment, the dispersion and compatibility of GO became better. The prepared sample was soaked in 3.5 wt% sodium chloride solution for 100 days; the modulus value at 0.01 Hz only dropped to 5.36×10^9 Ω cm^2, which was higher than that of 8.3×10^8 Ω cm^2 of unmodified GO-based coating[14]. Wang *et al.* used the π-π interaction between lignin and graphene to improve the stability and dispersion of graphene, thus synergistically enhancing the anticorrosive properties of coatings. When the addition of modified graphene was 0.5 wt%, the coating resistance (R_c) and charge transfer resistance (R_{ct}) were one to two orders of magnitude higher than that of the pure epoxy coating[15]. However, although the modification of GO by lignin can help improve its dispersibility and compatibility, the mechanism of its corrosion protection is relatively simple. Therefore, in order to achieve multiple anticorrosion properties of the coating and extend the service life of the metal, further modification of GO is needed.

The loading of corrosion inhibitors on GO is an effective means to endow coatings with self-healing properties[16-18]. When the corrosive medium spreads to the coating/metal interface causing metal corrosion, the corrosion inhibitor is excited and forms a dense protective layer on the metal surface, which prevents the metal from being damaged by deep corrosion[19]. Zinc ions are a kind of highly efficient cathode

anticorrosion inhibitor, which are widely used because of their low price[20] and excellent ability to isolate metals from corrosive substances. In the study by Mohammadkhani *et al.*, zinc ions were loaded onto polypyrrole-modified GO to design a composite coating with self-healing anticorrosion properties[2]. It had been demonstrated through electrochemical impedance spectroscopy, pull-out spectroscopy, and salt spray that the presence of zinc ions was beneficial to improve the anticorrosion performance of coatings.

In previous studies, we had studied the synergistic anticorrosion effect of nano-diamond and GO, and achieved good research results. However, the coating properties prepared in previous studies were relatively simple, lacked performance in photothermal conversion properties, and did not have good self-healing properties, which further limited its application. This work was based on the previous knowledge of anticorrosion, and by designing the molecular structure of the coating, it endowed the coating with various properties. Therefore, this work proposed a new strategy of graft modification of GO using lignin with active ester structure. The lignin was covalently attached to GO through a chemical reaction between the active ester and the epoxy group on GO. One step further, zinc ions were loaded onto lignin/GO through electrostatic interactions and combined with resin to obtain lignin/GO-based coatings with self-healing anticorrosion function. The loading of zinc ions on lignin/GO was verified by electron microscopy. The anticorrosive properties of lignin/GO-based coatings and scratch coatings were evaluated by electrochemical testing methods. The photothermal conversion performance of the coating was recorded and analyzed by a thermal imager. All in all, this research opened a new path for designing coatings with excellent photothermal conversion and self-healing anticorrosion properties. In addition, it had also sparked new design inspiration for lignin grafting modified GO.

EXPERIMENTAL SECTION

Raw materials

Epoxy resin came from Shandong Yousuo Chemical Technology Co., Ltd. Bamboo lignin (L) was provided by Guangzhou Yingding Biotechnology Co., LTD. GO was derived from previous preparation methods[21]. Triethylamine (Et_3N) and tetrahydrofuran (THF) were purchased from Tianjin Fuyu Fine Chemical Co., Ltd. Acetyl chloride, 4-dimethylaminopyridine (DMAP), N, N-dimethylformamide (DMF), sodium hydroxide (NaOH) and zinc nitrate hexahydrate ($Zn(NO_3)_2{\cdot}6H_2O$) came from Shanghai Aladdin Biochemical Technology Co., Ltd. Hydrochloric acid (HCL) came from Guangzhou Chemical Reagent Factory. Styrene came from Tianjin Yongda Chemical Reagent Co., Ltd. Cobalt naphthenate and 2-butanone peroxide came from Guangdong Meiheng New Material Technology Co., Ltd., China.

Preparation of lignin with active ester structure

First, 5.00 g lignin was dissolved in 100 mL THF and added to the flask with 11.4 mL Et_3N. The mixed solution was then transferred to an ice water bath and stabilized for 10 min. Immediately after, 8.5 mL acetyl chloride dissolved in 20.0 mL THF was dropped into the mixture and stirred at room temperature for 48 h. After completing the above steps, the pH of the system was adjusted to 2 with 1 M HCL solution, and it was poured into 1,000 mL deionized water and stirred for 30 min. The solution was filtered, washed three times with deionized water, and the obtained filter cake was dried in a vacuum oven at 55 °C to obtain lignin with active ester structure (XL). The specific reaction principle was shown in Scheme 1A.

Modification of GO by XL and zinc nitrate hexahydrate

First, 0.2 g XL, 0.1 g GO, and 0.005 g DMAP were added to the flask and dissolved in 50 mL DMF. The mixture was stirred at 150 °C for 5 h, then centrifuged, washed with DMF and anhydrous ethanol, and freeze-dried to obtain the modified GO (LGO). The specific reaction principle was shown in Scheme 1B. Next, 0.1 g LGO was dispersed in 50 mL deionized water and ultrasonically dispersed for 10 min. Immediately afterward, 0.15 g $Zn(NO_3)_2{\cdot}6H_2O$ was added and pH was adjusted to 8 using NaOH (10 wt%)

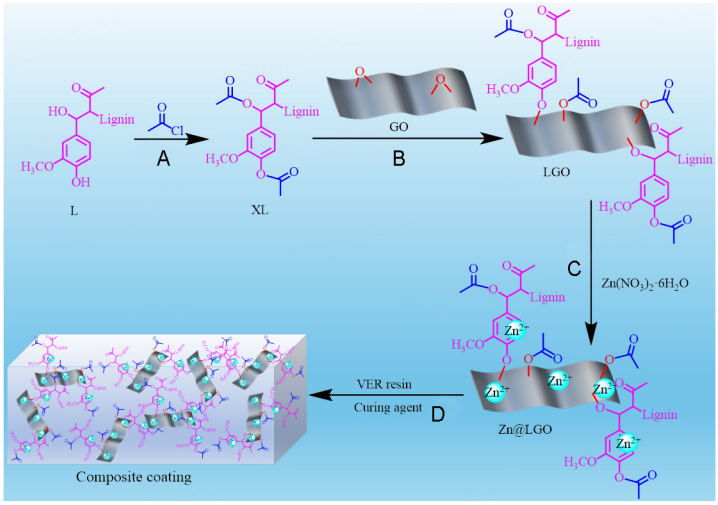

Scheme 1. Preparation of XL (A); modification of GO by XL (B); loading of zinc ions on LGO (C); preparation of lignin/GO-based coating (D).

solution. The mixture was reacted at 60 °C for 2 h. After all programs were completed, it was centrifuged, washed and filtered. The sample was dried at 60 °C for 24 h to obtain Zn@LGO. Please refer to Scheme 1C for the discussion process.

Preparation of lignin/GO-based coatings

Epoxy vinyl resin (VER) used was derived from previous preparation methods[21]. A mixture of 3.0 g VER and styrene (VER accounts for 70 wt%) was added to the glass bottle, followed by the addition of Zn@LGO (with amounts of 0.1, 0.2, and 0.4 wt%) and ultrasonically dispersed. Soon afterward, 0.3 wt% cobalt naphthenate and 1.0 wt% 2-butanone peroxide were added and mixed evenly. After coating the mixture on a clean steel plate, place it overnight in a 25 °C oven, and then heat it at 100, 130, 160, and 180 °C for 3, 2, 2, and 2 h. The coating thickness was around 45 microns. Please refer to Scheme 1D for detailed steps. Coating prepared with pure resin was labeled VER-0. Similarly, preparation coatings containing 0.1, 0.2 and 0.4 wt% Zn@LGO were labeled VER-1,VER-2 and VER-3, respectively. In this work, the composite coating was prepared by the thermal polymerization method, and the preparation process was relatively simple, easy to operate and large-scale preparation. In addition, in this work, lignin was used to modify GO, and the styrene used could participate in the polymerization reaction, which not only increased the added value of lignin and reduced the dependence on petroleum-based chemicals, but also avoided the volatilization of organic solvents, reducing the harm to construction personnel and the environment.

Characterizations

At room temperature, the functional groups of the powder samples were characterized by Fourier transform infrared spectroscopy (FTIR, Nicolet iS10) using KBr tablet method. The wavelength range was 4,000~500 cm^{-1}, the scanning times were 32 and the resolution was 4 cm^{-1}. The structure of the modified compounds was characterized by nuclear magnetic resonance (NMR) (AVANCE NEO 400 MHz) with dimethyl sulfoxide-d_6 (DMSO-d_6) as a solvent. The morphology of the sample was analyzed by scanning electron microscopy (SEM, SIGMA-300 ZEISS) at the accelerating voltage of 15 kV. The samples were tested after being sprayed with gold. The element content of the sample was detected by the attached energy dispersive spectrometer (EDS). A semi-quantitative analysis of the sample was performed using EDS and the sample was tested in a low vacuum mode of 5 keV. The test thickness of the sample was 0.45 mm; the take-off angle used was 35°, and the azimuth angle was 45°. The thermal degradation behavior of the sample

under nitrogen atmosphere was characterized using a thermogravimetric analysis (TGA, TG209F1LibraTM), with a heating rate of 10 °C/min. The crystal structure of the sample was characterized by X-ray diffraction (XRD, Ultima IV) at a scanning rate of 8°/min with Cu Kα radiation (λ = 0.154 nm) at room temperature. The measured diffraction angle ranged from 5° to 80°. The types and contents of elements on the surface of the sample were characterized by X-ray photoelectron spectroscopy (XPS, Thermo Scientific K Alpha). The excitation source was Al Kα radial, the beam spot was 400 μm, the operating voltage used was 12 kV, and the electron emission angle was 60°. The optimal energy resolution was 0.45 eV and the passing energy value was 1,486.6 eV. In the test, the combined energy of C1s = 284.80 eV was used for charge correction. When fitting, a nonlinear background subtraction method was used, and then new peaks were added to the peak fitting table as needed in the peak fitting mode while determining the range of spectral peak fitting. The photothermal conversion performance of the sample was evaluated by near infrared light source, and light intensity was 1.0 Wcm^{-2}. The adhesion strength between the coating and the steel plate was characterized by the automatic digital pull-out adhesion tester. The data used was the average value of three parallel tests. The hydrophilic and hydrophobic properties of the cured layer surface were characterized by special instruments, and the test was conducted at five different positions of the same sample. The average value was taken as the final contact angle value. Zetasizer (Nano ZS90, Malvern Instruments) was used to characterize the Zeta potential of the sample. The electrochemical impedance spectrum (EIS) of the sample was obtained by testing on the CHI-660E electrochemical workstation. During the test, the exposed area of the sample was 1 cm^2, the corrosive medium was 3.5 wt% brine, the Ag/AgCl electrode was used as the reference electrode, and the platinum sheet was used as the counterelectrode.

RESULTS AND DISCUSSION

Validation test for active esterified lignin

The FTIR analysis results for L and XL were displayed in Figure 1A. For L, the strong peak at 3,440 cm^{-1} was the characteristic peak of hydroxyl groups on L[22]. After L was esterified, its main characteristic peaks were detected on XL. The strength of hydroxyl peak on XL weakened and increased to 3,457 cm^{-1}, which was due to the depletion of hydroxyl group on lignin and the decrease of intermolecular hydrogen bond interaction. In addition, a new ester group peak appeared at 1,765 cm^{-1}, which was the result of esterification of the lignin. In Figure 1B, the main proton hydrogen on L was detected on XL. The new peak at δ = 2.0 ppm for XL was the methyl proton peak on acetyl chloride. Moreover, the phenolic hydroxyl proton peak (δ = 10.0 ppm) on L was not detected on XL, indicating that phenolic hydroxyl groups on L were fully involved in the esterification reaction. Please refer to Figure 1C for the results of analyzing the elemental content on L and XL using EDS. For L, its surface contained 81.5% carbon and 18.5% oxygen. However, the carbon content on the XL surface decreased to 76.7%, and oxygen content rose to 23.3%. This was the result of grafting acetyl chloride monomer onto XL. The above analysis confirmed that XL had been successfully prepared.

Validation test for modified GO

Please refer to Figure 1D for the heating state of modified GO in a nitrogen atmosphere. Mass loss of the sample within 200 °C was caused by water molecules adsorbed. In 200 to 400 °C, the degradation of GO was significant due to the presence of more oxygen-containing functional groups on its surface[23]. As the temperature increased, its mass was continuously lost. At 800 °C, its residual carbon ratio was 57.9 wt%. GO was modified, and its mass loss at the same temperature was reduced. At 800°C, the residual carbon ratios of LGO and Zn@LGO were 59.2 wt% and 69.0 wt%, indicating that the thermal stability of modified GO was improved. The Zeta potential of modified GO dispersion (0.2 mg/mL) was shown in Figure 1E; the Zeta potential of GO was -2.92 mV, indicating that GO showed electronegativity, which was caused by the carboxyl groups on its surface. For XL, its Zeta potential was -42.2 mV, and after GO was modified by XL,

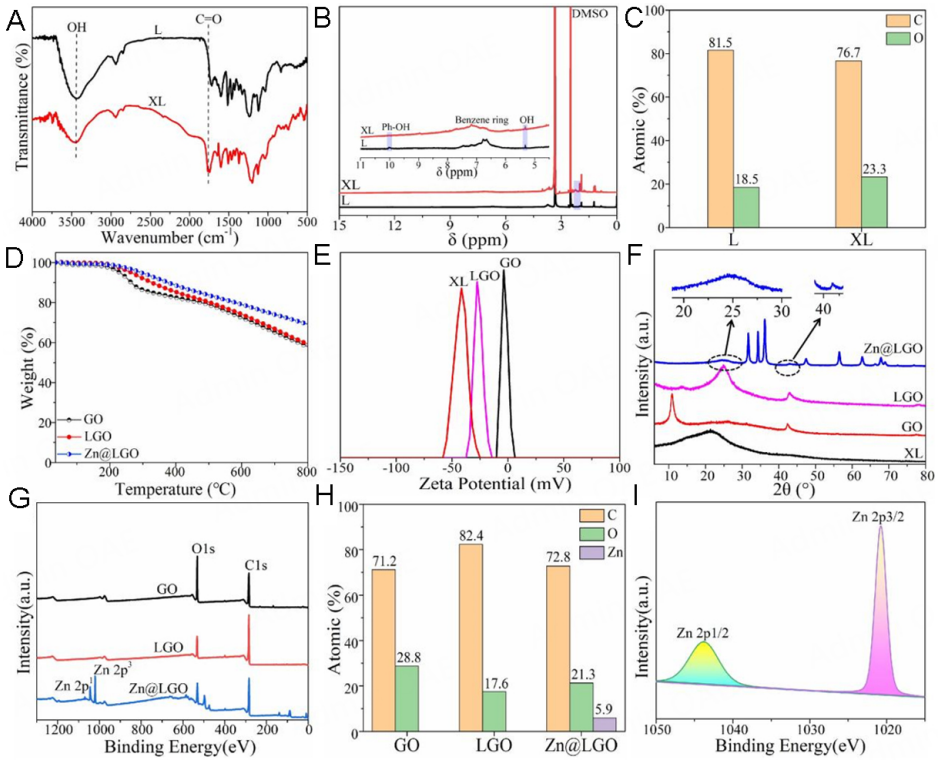

Figure 1. Infrared spectrum (A), ^{1}H-NMR spectrum (B), element content (C) of L and XL; thermal degradation curves of GO, LGO, Zn@LGO (D); Zeta potentials of XL, GO, LGO (E); XRD spectrum of XL, GO, LGO, Zn@LGO (F); XPS spectra (G) and elemental content (H) of GO, LGO, Zn@LGO; Zn XPS spectra of Zn@LGO (I).

the Zeta potential of LGO was -26.4 mV, which was also electronegativity. This indicated that the loading of zinc ions on LGO could be achieved through electrostatic interaction. The XRD results of the modified GO and XL were displayed in Figure 1F. For XL, it showed a wide diffraction peak at 21.4°, indicating that XL was an amorphous material. GO exhibited its corresponding (001) and (100) diffraction peaks at positions 11.0° and 42.4°[21]. After GO was modified by XL, the crystal plane at (001) disappeared, and a wide diffraction peak appeared at 24.8°, which was caused by the group reaction on GO with XL to reduce the oxygen-containing functional group, indicating that the structure of the modified GO had changed. After loading zinc ions onto LGO, the characteristic peak of LGO was retained at Zn@LGO, indicating that the loading of zinc ions did not affect the crystal structure of LGO. New diffraction peaks appeared at 31.6°, 34.3°, 36.2°, 47.3°, 56.4°, 62.7°, 66.3°, 67.8°, and 69.2°, which were (100), (002), (101), (102), (110), (103), (200), (112), and (201) planes of zinc oxide. From Figure 1G, the peak at 283.5 eV was attributed to C1s, while the peak at 530.4 eV was attributed to O1s. From Figure 1H, GO contained only carbon and oxygen elements, whose content was 71.2% and 28.8%, respectively. After XL was grafted onto GO, no new elements were introduced to LGO, but the carbon content increased to 82.4% and the oxygen content decreased to 17.6%. When zinc ions were loaded onto LGO, the zinc element was detected on Zn@LGO with a content of 5.9%. From Figure 1I, the zinc element in Zn@LGO was deconvoluted into Zn 2p3/2 (1,022.2 eV) and Zn 2p1/2 (1,045.1 eV)[24], indicating that the valence of zinc in Zn@LGO was positive 2. The morphological changes of GO during the modification process were characterized using SEM. From Figure 2A, there was an obvious enrichment phenomenon in GO. This phenomenon was closely related to the strong intermolecular forces between GO. After grafting XL onto GO, the dispersibility of LGO was effectively improved, and lignin was observed on GO surface [Figure 2B]. In Figure 2C, there were more granular substances on GO, which were zinc oxide crystals. EDS was used to conduct element analysis and

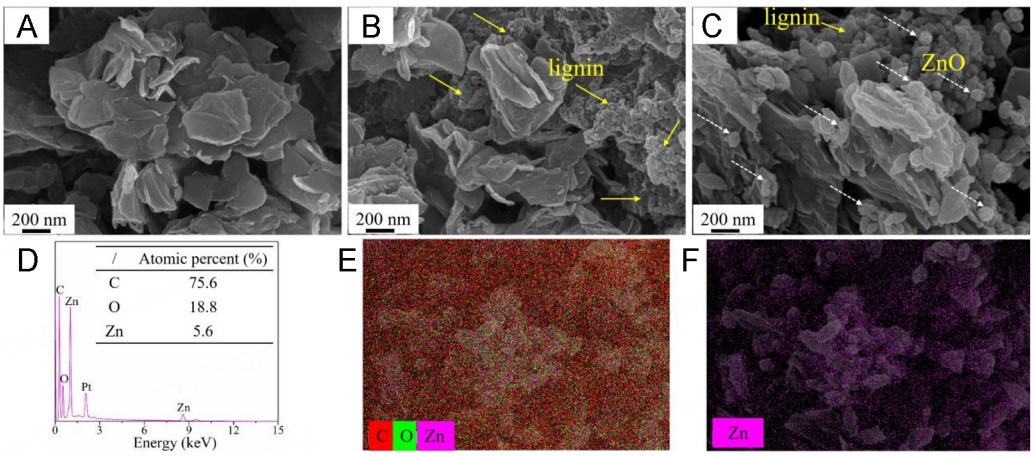

Figure 2. SEM images of GO (A), LGO (B), and Zn@LGO (C); surface element content (D), Mapping diagram (E) and Zn distribution diagram (F) of Zn@LGO.

Mapping scanning on Zn@LGO surface, and 5.6% zinc element was detected in Figure 2D and E. Besides, the zinc element was evenly dispersed on GO [Figure 2F]. The above analysis confirmed that Zn@LGO was obtained.

Morphology, adhesion strength, contact angle (CA), and photothermal conversion properties of composite coatings

The dispersion states of the resins and resins containing different Zn@LGO contents were listed in Figure 3A-D. From Figure 3A, the resin had good fluidity, and less resin remained on the bottle wall after being placed in different positions. From Figure 3B-D, after ultrasonic treatment, different contents of Zn@LGO were well dispersed in resin, and the mixture could flow well after being placed in different positions. This would facilitate the coating and casting of the mixture on the metal surface. The dispersion state of Zn@LGO in cured coating was characterized by SEM, and the fracture morphology of cured coating was exposed in Figure 3E-H. From Figure 3E, the fracture surface of coating VER-0 was relatively flat and smooth. From Figure 3F-H, Zn@LGO was observed on the fracture surface, and Zn@LGO was embedded in resin, indicating that there was a good interface interaction between Zn@LGO and resin. Adhesion strength of cured coatings on the metal surface was obtained by pull-out device. From Figure 4A, the adhesion strength of coating VER-0 was 1.15 MPa, which was caused by the mechanical interlocking, van der Waals forces and hydrogen bonds between the resin and metal interface. After adding Zn@LGO to resin, adhesion strength of the coating was improved, and corresponding adhesion strength of cured coatings VER-1, VER-2, and VER-3 was increased to 1.56, 1.82 and 2.18 MPa. This was attributed to excellent interfacial compatibility between Zn@LGO and resin, the intermolecular interaction formed by polar groups on Zn@LGO and metal surface. The fine interface between Zn@LGO and resin facilitated the transfer of loads from matrix to Zn@LGO, thereby preventing separation of the coating from metal interface. The CA value could be used to characterize the hydrophilic/hydrophobic properties of the coating surface, and the results were shown in Figure 4B. For the coating formed by pure resin, the CA value on the surface of VER-0 was the smallest, only 51.2°, which was a hydrophilic surface. When Zn@LGO was introduced into the cured coating, the CA value of all coating surfaces was improved. When the amount of Zn@LGO added was 0.4 wt%, the CA value of the surface of coating VER-3 was 91.5°, reaching the standard of a hydrophobic surface. Photothermal conversion performance of cured coatings was investigated through near-infrared irradiation (NIR) on the coating surface. The temperature changes of cured coatings under NIR at different times were displayed in Figure 4C, and the infrared thermal images of cured coatings after being irradiated for 180 s were exposed in Figure 4D-G. From Figure 4C, the temperature of the cured

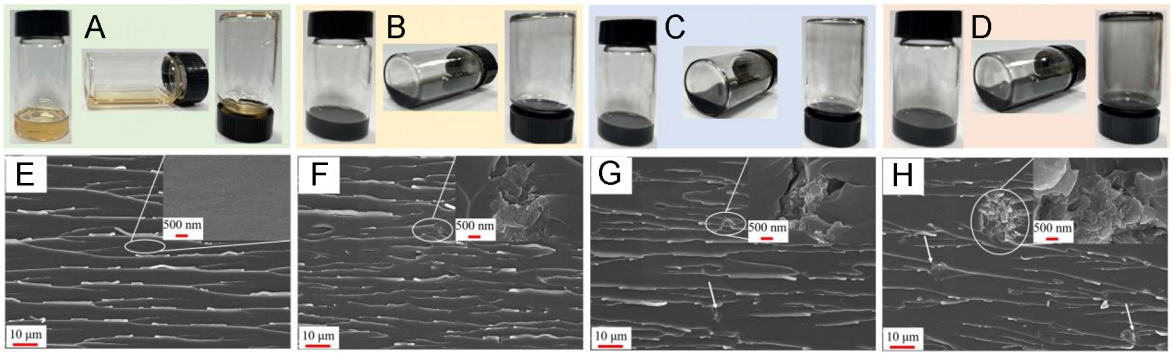

Figure 3. State of epoxy resin (A); dispersion state of 0.1 wt% (B), 0.2 wt% (C), and 0.4 wt% (D) Zn@LGO in resin; cross-sectional morphology of coatings VER-0 (E), VER-1 (F), VER-2 (G), and VER-3 (H).

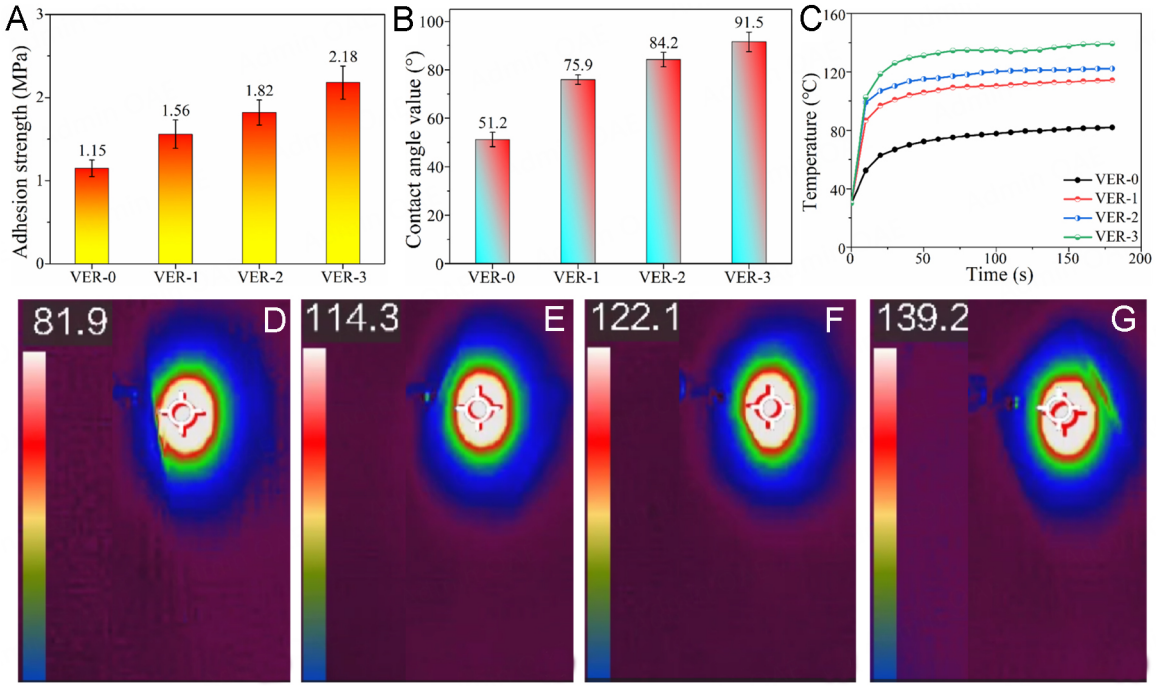

Figure 4. Adhesion strength of coatings on metal surfaces (A), contact angle of coatings (B), surface temperature of coatings under 980 nm NIR light irradiation for 180 s (C), and real-time temperature images of coatings (D) VER-0, (E) VER-1, (F) VER-2, and (G) VER-3 at 180 s.

coating surface increased rapidly within 30 s of radiation, after which the temperature basically remained unchanged. For coating VER-0, even if it was radiated for 180 s, its surface temperature was only 81.9 °C. When 0.1, 0.2, and 0.4 wt% Zn@LGO were added to resin, the surface temperature of the cured coating increased significantly. After 180 s of radiation, the surface temperatures of cured coatings VER-1, VER-2, and VER-3 coatings reached 114.3, 122.1 and 139.2 °C. The result was due to the inherent photothermal conversion capability of GO, which could convert light energy into heat energy[25]. With the rise of Zn@LGO content, the content of GO in the coating increased, resulting in better photothermal conversion performance of the coating under NIR radiation.

Anticorrosion performance of cured coatings

EIS is used to evaluate the anticorrosion performance of protective coatings[26,27], and the protective performance data of the coating obtained on this basis were exposed in Figure 5. In the Bode curves, the modulus value at 0.01 Hz ($Z_{0.01Hz}$) is a method of judging the anticorrosion performance of the coating, and for the corrosion resistance of the coating, the greater the value, the more favorable the role of the protective coating[28,29]. From Figure 5A, D, G, and J, Figure 6A, the $Z_{0.01Hz}$ values of all coatings decreased with prolonged immersion time in 3.5 wt% saltwater, indicating that the anticorrosion performance of coatings was closely related to their service life. The initial $Z_{0.01Hz}$ values of all coatings were approximately 3.4×10^{10} Ω cm^2. During the immersion of the coating in salt water, the modulus value of the cured layer VER-0 decreased significantly at 0.01Hz. After 100 days, the $Z_{0.01Hz}$ value of coating VER-0 decreased to 5.0×10^7 Ω cm^2, indicating that the corrosion resistance of the coating was greatly weakened. After adding Zn@LGO to the resin, the $Z_{0.01Hz}$ value change of the corresponding coating gradually increased, indicating that the anticorrosion performance of the coating had been improved. The protective ability of cured coating was enhanced with the increase of Zn@LGO content, which reflected that the anticorrosive property of the cured coating was closely related to the amount of anticorrosive filler added. Among them, coating VER-3 had the highest $Z_{0.01Hz}$ value, indicating that protective ability of cured coating VER-3 was the best. Even the cured coating VER-3 was placed in a 3.5 wt% sodium chloride solution for 100 days, $Z_{0.01Hz}$ value of cured coating VER-3 remained at 1.3×10^9 Ω cm^2, which was two orders of magnitude higher than coating VER-0. In the study of Ma *et al.*, compound polydopamine, GO and mesoporous silica nanoparticles loaded with benzotriazole were added to epoxy resin to prepare a composite coating with self-healing anticorrosion properties[17]. After soaking in 3.5 wt% NaCl solution for 30 days, the impedance modulus of the coating at the low frequency decreased to 1.42×10^7 cm^2, which was much lower than that of the coating prepared in this work (100 days, 1.3×10^9 Ω cm^2). This indicated that the coatings prepared in this work had relatively excellent anticorrosion properties. In addition, the lignin and zinc nitrate used in this work also had the advantages of green, environmental protection and low price, which provided a reference for the preparation of low-cost, green economy and high-efficiency anticorrosive composite coatings.

The phase angle diagram is also an important basis for evaluating the protection performance of cured coatings, and the characterization results were shown in Figure 5B, E, H, K. At the beginning of immersion, all coatings had a wide plateau and a high absolute phase angle at high frequencies. As the coating was soaked over time, the platform of the coating at high frequencies gradually narrowed, and the absolute value of the phase angle decreased, which was a manifestation of the deterioration of the coating's anticorrosion performance. Researchers typically use a break point frequency at -45° (f_b) to qualitatively evaluate the corrosion resistance of coatings, if the f_b value is large, it indicates that the coating delamination is severe, which in turn determines that the anticorrosion performance of the coating is poor, and its value was shown in Figure 6B. In the initial stage, the f_b values of cured coatings VER-0, VER-1, VER-2, and VER-3 were 0.0331, 0.0209, 0.0166, and 0.0110 Hz, respectively. After immersing the cured coating in a 3.5 wt% aqueous solution of sodium chloride, their f_b values gradually moved to high frequency, indicating that the interface between the coating and metal was increasingly stratified. The coating was placed in saltwater for 100 days, and the f_b values of cured coatings VER-0, VER-1, VER-2, and VER-3 decreased to 9.3325, 0.2000, 0.1738, and 0.1259 Hz. By comparison, there was a serious delamination phenomenon between coating VER-0 and the metal interface, which was one of the reasons why the protective ability of cured coating VER-0 was greatly weakened during long-term use. On the contrary, after adding Zn@LGO into resin, the f_b value was relatively small, indicating that adding functional fillers to resin was a feasible method to improve the corrosion resistance of the coating. The change of impedance arc radius in Nyquist diagram can also indirectly reflect the anticorrosive property of the coating. If the impedance arc radius is large, it is considered that the anticorrosion performance of the coating is good[30]. From the Nyquist plots in Figure 5C, F, I, L, it could be seen that with the passage of time, the impedance arc radius of all cured

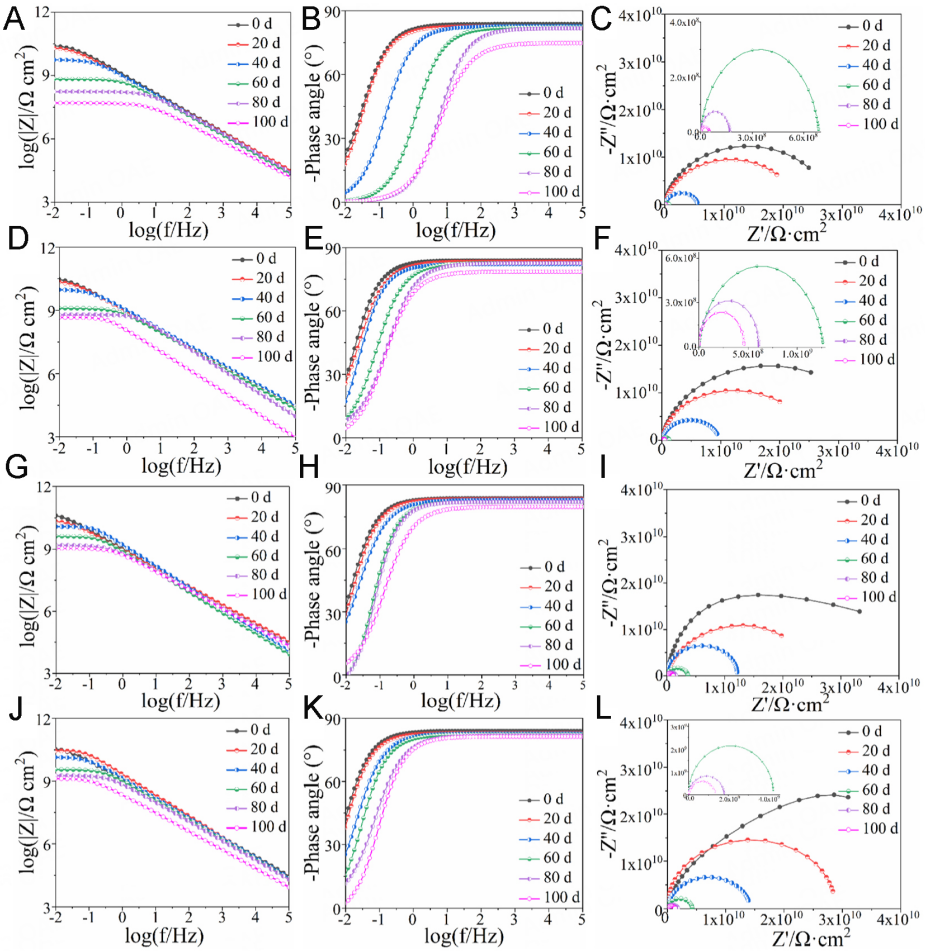

Figure 5. Bode curves, phase angle curves, and Nyquist curves of cured coatings VER-0 (A-C), VER-1 (D-F), VER-2 (G-I), and VER-3 (J-L) during placed in a 3.5 wt% sodium chloride solution for 100 days.

coatings placed in salt water gradually decreased, so it could be judged that the corrosion resistance of the coating was weakening. By comparison, the impedance arc radius of the coating after adding Zn@LGO was higher than coating VER-0, indicating that addition of Zn@LGO was beneficial for improving anticorrosion performance of the coating. The relationship between the impedance arc radius during the soaking test time was VER-0 < VER-1 < VER-2 < VER-3; obviously, the anticorrosion performance of cured coating VER-3 was the best.

The obtained electrochemical data circuit was fitted, and the obtained R_c was displayed in Figure 6C. Similarly, the larger the R_c value, the better the corrosion resistance of the coating. When the initial coating was soaked, the R_c values of cured coatings VER-0, VER-1, VER-2, and VER-3 were 2.79×10^{10}, 3.64×10^{10}, 5.50×10^{10}, and 6.90×10^{10} Ω cm^2. When the cured coating was placed in an aqueous solution of 3.5 wt% sodium chloride for 100 d, the R_c values of all samples showed an obvious decreasing trend, but its value was always VER-0 < VER-1 < VER-2 < VER-3. When the coating was soaked for 100 days, the R_c values of cured coatings VER-0, VER-1, VER-2, and VER-3 were 5.00×10^{7}, 4.50×10^{8}, 1.10×10^{9}, and 2.90×10^{9} Ω cm^2. For cured coating VER-0, its R_c was reduced by three orders of magnitude, indicating that its coating had the worst corrosion resistance. Obviously, adding Zn@LGO to resin could still increase the R_c value and improve the corrosion resistance of the coating. By numerical comparison, the R_c value of cured coating

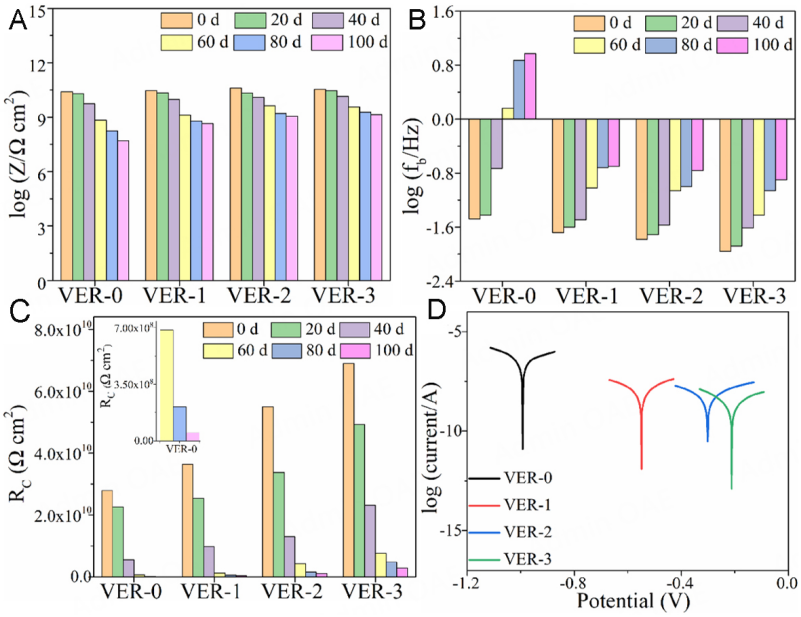

Figure 6. Modulus values of coatings at low frequencies (A), f_b values of coatings (B), coating resistance of coatings (C), and Tafel polarization curves (D) of coatings soaked in 3.5 wt% saline for 100 days.

VER-3 was two orders of magnitude higher than that of VER-0, which showed better anticorrosion performance.

The dynamic potential polarization test was conducted on the coating soaked in salt water for 100 days, and the results were shown in Figure 6D and Table 1. It is generally agreed that coatings with good anticorrosion performance often had lower corrosion current density and higher corrosion potential[31]. The corrosion current density and corrosion potential of coating VER-0 were 6.20 × 10^{-7} A cm^2 and -0.99 V. When Zn@LGO was added to resin, the corrosion current density decreased and the corrosion potential increased, indicating that the protection performance of the coating was enhanced. When the addition of Zn@LGO was 0.4 wt%, the corrosion current density and corrosion potential became 3.26 × 10^{-9} A cm^2 and -0.21 V. This showed that the cured coating VER-3 still had good anticorrosion properties even if it was soaked in salt water for 100 days. The protection efficiency of cured coatings is calculated by Formula (1).

$$\text{Protective efficiency (\%)} = (i_{blank} - i)/i_{blank} \times 100\% \quad (1)$$

From Table 1, the protection efficiency of cured coatings increased with the Zn@LGO content, from 97.7% to 99.5%, indicating that the content of Zn@LGO was one of the main factors affecting the corrosion resistance of the coating. The coating on the metal surface was removed to observe the corrosion phenomenon on the metal surface. From Figure 7A and B, the metal surface under the cured coating VER-0 contained lots of corrosion products. EDS analysis showed that the surface contained 0.5% chlorine and 41.3% oxygen elements. This reflected that the cured coating would lose its ability to protect the metal after a long time of infiltration, and the result was that the corrosive medium spread to the metal surface, causing metal corrosion. From Figure 7C and D, Figure 7E and F, and Figure 7G and H, after adding Zn@LGO to resin, the metal corrosion phenomenon under the corresponding coating was gradually suppressed, especially when the content of Zn@LGO was 0.4 wt%, fewer corrosion products were observed on the metal surface protected by the cured coating VER-3. It could also be clearly observed from the elemental content

Table 1. EIS data and protective efficiency of cured coatings in 3.5 wt% sodium chloride solution for 100 days

Samples	i (A cm^2)	E (V)	Protective efficiency (%)
VER-0	6.20×10^{-7}	-0.99	/
VER-1	1.44×10^{-8}	-0.55	97.7
VER-2	7.35×10^{-9}	-0.30	98.8
VER-3	3.26×10^{-9}	-0.21	99.5

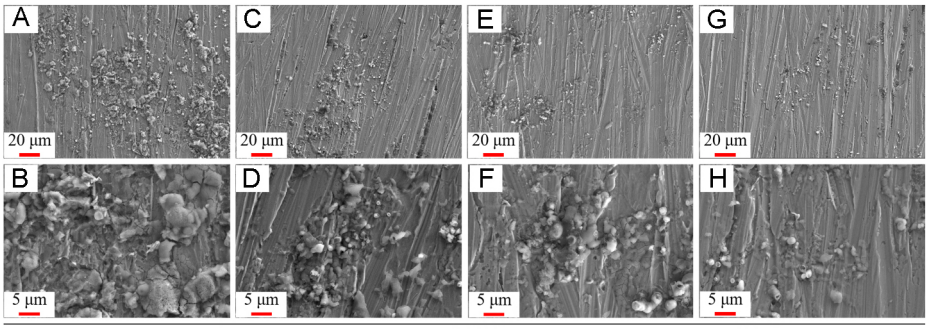

	Atomic (%)		
Samples	O	Cl	Fe
VER-0	41.3	0.5	58.2
VER-1	34.9	0.3	64.8
VER-2	18.8	0.2	81.0
VER-3	13.8	0.1	86.1

Figure 7. Corrosion morphology and elemental composition of metals under coatings VER-0 (A and B), VER-1 (C and D), VER-2 (E and F), and VER-3 (G and H).

in Figure 7 that elemental content of chlorine and oxygen elements on the metal surface under the cured coatings VER-1, VER-2, and VER-3 had decreased to 0.3% and 34.9%, 0.2% and 18.8%, 0.1% and 13.8%. The chlorine element came from brine, and the higher the chlorine content, the more serious the penetration of the coating by brine. In a word, cured coating VER-3 had the strongest ability to block the intrusion of corrosive media, and its anticorrosion performance was optimal within the same soaking time.

Through the above analysis, it could be concluded that the anticorrosion performance of the coating was time-dependent, and its protective performance against metals decreased over long-term use. The weakening of anticorrosion performance was mainly related to the following factors: (1) when the coating was soaked for a long time, the corrosive medium would reach the interface between the coating and the metal, which would cause metal corrosion; (2) there were ester groups in the resin, which would degrade during long-term use, resulting in changes in the structure of the coating and weakening of its protective ability; (3) in long-term use, the alkaline environment provided by the generated hydroxide ions or the corrosion products generated would lead to the weakening of the adhesion between the coating and the metal, which would accelerate the intrusion of the corrosive medium, resulting in metal corrosion. In order to enhance the anticorrosion properties of the coating, it was necessary to increase the cross-linking density of the coating to improve its compactness, modify the epoxy resin to introduce monomers with fewer ester groups, or apply special treatments of the metal surface to increase its adhesion to the coating.

Self-healing anticorrosion properties of cured coatings

In order to study the self-healing anticorrosion properties of the cured coating, the coating was scratched with a sharp blade. Figure 8 showed the Bode plots, $Z_{0.01Hz}$ values, R_{ct} and surface morphology of the scratch

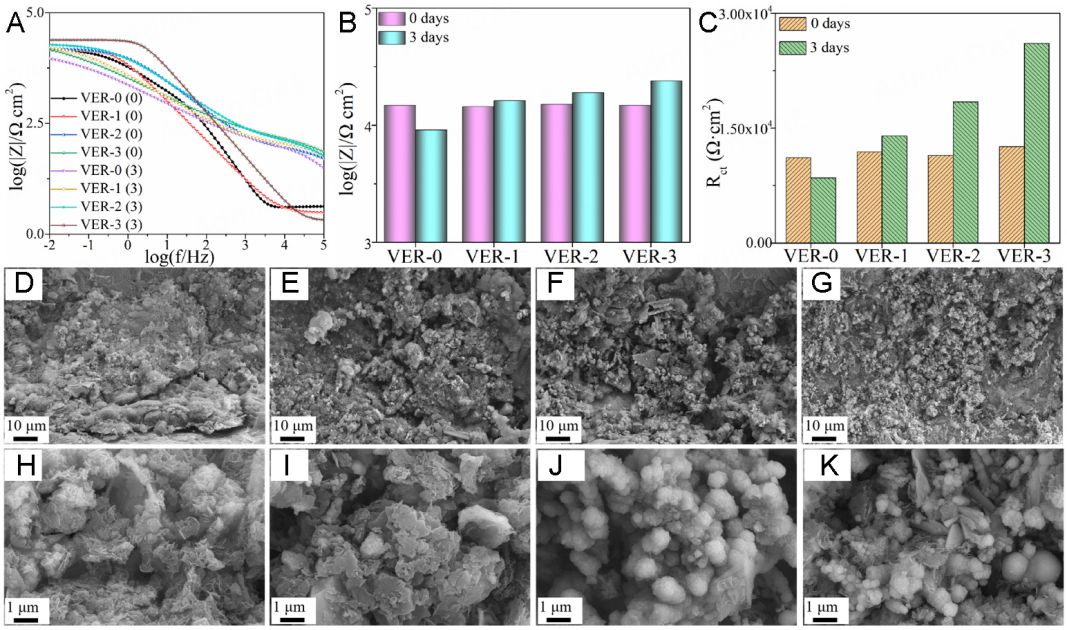

Figure 8. Bode plots (A), $Z_{0.01Hz}$ values (B), and R_{ct} values (C) of the scratched coating soaked in 3.5 wt% saline for day 0 and day 3; morphology of scratch coating VER-0 (D and H), VER-1 (E and I), VER-2 (F and J), and VER-3 (G and K) after placed in a 3.5 wt% sodium chloride solution for 3 days.

coating after soaking in 3.5 wt% brine for three days. From Figure 8A and B, after the coating was scratched, its $Z_{0.01Hz}$ value was basically maintained at about 1.48×10^4 Ω cm². When the scratch cured coating was placed in 3.5 wt% sodium chloride solution for three days, $Z_{0.01Hz}$ value of cured coating VER-0 was reduced to 9.12×10^3 Ω cm², indicating that the scratch coating VER-0 basically lost its protective effect. On the contrary, the $Z_{0.01Hz}$ values of cured coatings VER-1, VER-2, and VER-3 were increased, indicating that although the coating was scratched, its corrosion resistance during the immersion process was enhanced. Among all the samples tested, coating VER-3 had the largest $Z_{0.01Hz}$ value, which was 2.40×10^4 Ω cm². R_{ct} was used to characterize the corrosion resistance of scratch coating. The higher the value, the stronger the corrosion resistance of the coating. From Figure 8C, after soaking the scratched coating for three days, the R_{ct} value of coating VER-0 decreased from 1.12×10^4 to 8.50×10^3 Ω cm². For coatings VER-1, VER-2, and VER-3, the R_{ct} value was increased to 1.40×10^4, 1.84×10^4, and 2.61×10^4 Ω cm². After the coating was mechanically removed from the metal surface, lots of loose porous corrosion products were observed on the metal surface under coating VER-0 [Figure 8D and H]. However, on the metal surface protected by cured coatings VER-1, VER-2 and VER-3, a dense product was formed, which effectively isolated the contact between the corrosive medium and the metal, resulting in a coating with high $Z_{0.01Hz}$ and R_{ct} values. Through analysis, it could be concluded that coating VER-0 did not possess self-healing anticorrosion properties, while adding Zn@LGO to resin could endow the coating with better self-healing anticorrosion properties. This self-healing anticorrosion performance was related to the amount of Zn@LGO added, and the more Zn@LGO was added, the better the self-healing anticorrosion performance of the coating.

Self-healing anticorrosion mechanism of composite coatings

For the pure resin coating (VER-0), the corrosive medium (H_2O, O_2 and Cl^-) uses the microdefects in the coating to diffuse into the interior of the coating, reaching the metal-coating interface in a short time, and causing chemical corrosion of the metal. After adding Zn@LGO to the resin, the coating was self-healing, which could improve its long-term corrosion resistance by repairing defects in the coating or isolating the contact between the corrosive medium and the metal, and its mechanism was shown in Figure 9. On the

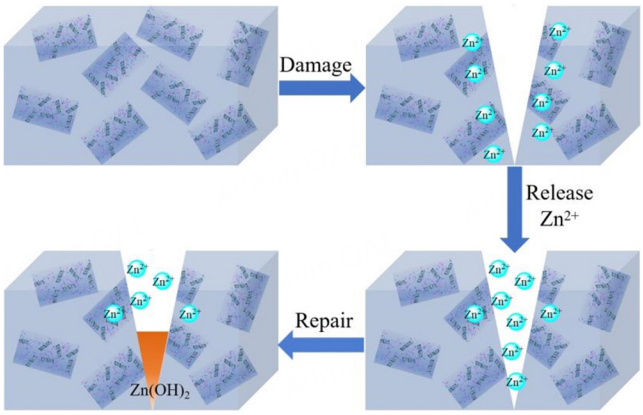

Figure 9. Self-healing anticorrosion mechanism of coatings.

one hand, the nanomaterials contained in the coating could make the path of diffusion of the corrosive medium more tortuous, and the corrosive medium could not contact the metal in the short term, thus extending the service life of the metal. In addition, after metal corrosion, hydroxide ions would be produced in the cathode ($O_2 + 2H_2O + 4e \rightarrow 4OH^-$), which combined with the zinc ions released on Zn@LGO to form zinc hydroxide [$Zn^{2+} + 2OH^- = Zn(OH)_2$] and coated metal defects or corroded areas. The dense protective layer of hydroxide formed by this self-healing process would isolate the corrosive medium from the metal and prevent further corrosion of the metal. It was precisely because the composite coating had the synergistic effect of "active anticorrosion" and "passive anticorrosion" that the coating showed better anticorrosion properties.

CONCLUSION

In this work, lignin with active ester structure was prepared by esterification reaction, and then graft-modified onto GO. Finally, modified GO loaded with zinc ions was added to the resin to prepare the self-healing anticorrosion composite coating. The results showed that the adhesion strength of the coating to the metal surface and the contact angle of the coating surface were improved by adding Zn@LGO to the resin. In addition, introducing Zn@LGO into the resin also endowed the coating with photothermal conversion performance. When the coating was irradiated with NIR for 180 s, the temperature could reach as high as 139.2 °C. Electrochemical testing showed that the addition of Zn@LGO to the resin had a significant impact on the anticorrosion performance of coatings. When the cured coating was placed in 3.5 wt% sodium chloride solution for 100 days, $Z_{0.01Hz}$ value of the cured coating VER-3 reached 1.3×10^9 Ω cm^2, which was two orders of magnitude higher than that of pure resin coating. The scratch test confirmed that the presence of Zn@LGO could endow the coating with self-healing anticorrosion properties. Among them, when the content of Zn@LGO was 0.4 wt%, the self-healing anticorrosion properties of coating VER-3 were the best. In summary, this work not only enhanced the added value of biomass materials, but also provided new research ideas for the preparation of composite coatings with self-healing, anticorrosion, and photothermal conversion properties.

DECLARATIONS

Authors' contributions

Experiment implementation, data acquisition and interpretation, statistical analyses, conceptualization, manuscript writing, funding acquisition: Xu, C.

Conceptualization, study design, interpretation, manuscript review and editing: Liang, W.

Discussion, methodology, manuscript revision: Hong, P.; Hu, Y.
Data interpretation, supervision, manuscript review, funding acquisition: Yang, Z.; Pang, H.

Availability of data and materials

The data that support the findings of this study are available from the corresponding author upon reasonable request.

Financial support and sponsorship

This work was supported by the Guangdong Basic and Applied Basic Research Foundation (2023A1515110462), the GDAS' Project of Science and Technology Development (2022GDASZH-2022010109, 2020GDASYL-20200102029), and the Science & Technology Program of Guangdong Province (2022A0505050062, 2023B0101020002).

Conflicts of interest

All authors declared that there are no conflicts of interest.

Ethical approval and consent to participate

Not applicable.

Consent for publication

Not applicable.

REFERENCES

1. Zhu, X.; Yan, Q.; Cheng, L.; Wu, H.; Zhao, H.; Wang, L. Self-alignment of cationic graphene oxide nanosheets for anticorrosive reinforcement of epoxy coatings. *Chem. Eng. J.* **2020**, *389*, 124435. DOI
2. Mohammadkhani, R.; Ramezanzadeh, M.; Saadatmandi, S.; Ramezanzadeh, B. Designing a dual-functional epoxy composite system with self-healing/barrier anti-corrosion performance using graphene oxide nano-scale platforms decorated with zinc doped-conductive polypyrrole nanoparticles with great environmental stability and non-toxicity. *Chem. Eng. J.* **2020**, *382*, 122819. DOI
3. Zafar, S.; Kahraman, R.; Shakoor, R. A. Silane functionalization of titania-graphene oxide nanocomposite for superior anticorrosion polyurethane coatings on steel. *Colloid. Surface. A.* **2024**, *703*, 135434. DOI
4. Jena, G.; Philip, J. A review on recent advances in graphene oxide-based composite coatings for anticorrosion applications. *Prog. Org. Coat.* **2022**, *173*, 107208. DOI
5. Wu, Y.; Wu, Y.; Sun, Y.; Zhao, W.; Wang, L. 2D nanomaterials reinforced organic coatings for marine corrosion protection: state of the art, challenges, and future prospectives. *Adv. Mater.* **2024**, *36*, e2312460. DOI
6. Ding, X.; Wang, Q.; Xu, X.; Nie, X.; Xu, X.; Li, J. A novel epoxy resin composite coating containing polyaniline modified GO with triple anti-corrosion effects of barrier, passivation and corrosion inhibition. *Prog. Org. Coat.* **2024**, *194*, 108564. DOI
7. Rabchinskii, M. K.; Ryzhkov, S. A.; Besedina, N. A.; et al. Guiding graphene derivatization for covalent immobilization of aptamers. *Carbon* **2022**, *196*, 264-79. DOI
8. Yang, Z.; Liu, B.; Yuwen, C.; et al. Preparation and performance studies of modified graphene oxide/polyaniline composite anticorrosive coatings. *Prog. Org. Coat.* **2024**, *197*, 108855. DOI
9. Li, X.; Gao, X.; Liu, J.; et al. Bi-functional epoxy coating with long-term protection for Q235 steel prepared by incorporating melamine-grafted and carbon-black-modified graphene oxide. *Surf. Coat. Technol.* **2024**, *485*, 130883. DOI
10. Ge, S.; Wei, K.; Peng, W.; et al. A comprehensive review of covalent organic frameworks (COFs) and their derivatives in environmental pollution control. *Chem. Soc. Rev.* **2024**, *53*, 11259-302. DOI
11. Cao, Y.; Liu, Z.; Zheng, B.; et al. Synthesis of lignin-based polyols via thiol-ene chemistry for high-performance polyurethane anticorrosive coating. *Compos. Part. B. Eng.* **2020**, *200*, 108295. DOI
12. Shi, Y.; Wu, M.; Ge, S.; et al. Advanced functional electromagnetic shielding materials: a review based on micro-nano structure interface control of biomass cell walls. *Nanomicro. Lett.* **2024**, *17*, 3. DOI PubMed PMC
13. Wang, J.; Seidi, F.; Shi, X.; Li, C.; Huang, Y.; Xiao, H. Unveiling the potential of dual-extrinsic/intrinsic self-healing lignin-based coatings for anticorrosion applications. *Int. J. Biol. Macromol.* **2025**, *285*, 138073. DOI

14. Xu, C. A.; Li, X.; Tong, Z.; et al. Mimosa inspired intelligent anti-corrosive composite coating by incorporating lignin and pyridine derivatives grafted graphene oxide. *Chem. Eng. J.* **2024**, *483*, 149316. DOI
15. Wang, S.; Hu, Z.; Shi, J.; et al. Green synthesis of graphene with the assistance of modified lignin and its application in anticorrosive waterborne epoxy coatings. *Appl. Surf. Sci.* **2019**, *484*, 759-70. DOI
16. Yu, X.; Zhang, M.; Chen, H. Superhydrophobic anticorrosion coating with active protection effect: graphene oxide-loaded inorganic/organic corrosion inhibitor for magnesium alloys. *Surf. Coat. Technol.* **2024**, *480*, 130586. DOI
17. Ma, Y.; Huang, H.; Zhou, H.; et al. Superior anti-corrosion and self-healing bi-functional polymer composite coatings with polydopamine modified mesoporous silica/graphene oxide. *J. Mater. Sci. Technol.* **2021**, *95*, 95-104. DOI
18. Habibiyan, A.; Ramezanzadeh, B.; Mahdavian, M.; Bahlakeh, G.; Kasaeian, M. Rational assembly of mussel-inspired polydopamine (PDA)-Zn (II) complex nanospheres on graphene oxide framework tailored for robust self-healing anti-corrosion coatings application. *Chem. Eng. J.* **2020**, *391*, 123630. DOI
19. Yimyai, T.; Crespy, D.; Rohwerder, M. Corrosion-responsive self-healing coatings. *Adv. Mater.* **2023**, *35*, e2300101. DOI PubMed
20. Gu, F.; Guo, W.; Yuan, Y.; et al. External field-responsive ternary non-noble metal oxygen electrocatalyst for rechargeable zinc-air batteries. *Adv. Mater.* **2024**, *36*, e2313096. DOI
21. Xu, C. A.; Chu, Z.; Li, X.; et al. Vanillin and organosilicon functionalized graphene oxide modified ester resin composite coatings with excellent anti-corrosion properties. *Prog. Org. Coat.* **2023**, *183*, 107804. DOI
22. Luo, Z. G.; Zhang, Y.; Wang, H.; et al. Modified nano-lignin as a novel biomass-derived corrosion inhibitor for enhanced corrosion resistance of carbon steel. *Corros. Sci.* **2024**, *227*, 111705. DOI
23. Sun, W.; Tang, E.; Zhao, L.; et al. The waterborne epoxy composite coatings with modified graphene oxide nanosheet supported zinc ion and its self-healing anticorrosion properties. *Prog. Org. Coat.* **2023**, *182*, 107609. DOI
24. Rabchinskii, M. K.; Sysoev, V. V.; Brzhezinskaya, M.; et al. Rationalizing graphene-ZnO composites for gas sensing via functionalization with amines. *Nanomaterials* **2024**, *14*, 735. DOI PubMed PMC
25. Fu, X.; Dou, H.; Fan, Y.; et al. Anticorrosion coating with near-infrared light triggered precisely controllable self-healing performances. *J. Colloid. Interface. Sci.* **2025**, *683*, 587-99. DOI
26. Ding, J.; Zhao, H.; Zhou, M.; Liu, P.; Yu, H. Super-anticorrosive inverse nacre-like graphene-epoxy composite coating. *Carbon* **2021**, *181*, 204-11. DOI
27. Wang, X.; Leng, W.; Nayanathara, R. M. O.; et al. Anticorrosive epoxy coatings from direct epoxidation of bioethanol fractionated lignin. *Int. J. Biol. Macromol.* **2022**, *221*, 268-77. DOI
28. Zhang, C.; Li, W.; Liu, C.; et al. Effect of covalent organic framework modified graphene oxide on anticorrosion and self-healing properties of epoxy resin coatings. *J. Colloid. Interface. Sci.* **2022**, *608*, 1025-39. DOI
29. Lei, Y.; Liu, Y.; Liu, Q.; et al. Nacre-mimetic strategy to fabricate waterborne FrGO/Zn/epoxy coatings with dual corrosion protection. *ACS. Appl. Mater. Interfaces.* **2023**, *15*, 28570-80. DOI
30. Zhu, Q.; Li, E.; Liu, X.; et al. Synergistic effect of polypyrrole functionalized graphene oxide and zinc phosphate for enhanced anticorrosion performance of epoxy coatings. *Compos. Part. A. Appl. Sci. Manuf.* **2020**, *130*, 105752. DOI
31. Li, F.; Sun, R.; Chen, K.; Gao, H. Improvement in adhesion and corrosion resistance of Ce-based coating on micro-arc oxidized AZ31B Mg alloy via employing graphene oxide as an effective interlayer. *Mater. Today. Commun.* **2024**, *40*, 109862. DOI